Ultra-bright biphoton emission from an atomic vapor based on Doppler-free four-wave-mixing and collective emission

Y. P. Huang and M. G. Moore

Department of Physics & Astronomy, Michigan State University, East Lansing, MI 48824
(Dated: January 30, 2009)

We propose a novel 'butterfly' level scheme to generate highly correlated photon pairs from atomic vapors. With multi-photon Doppler-free pumping, background Rayleigh scattering is dipole-forbidden and collective emission is permitted in all directions. This results in usable pairs generated simultaneously in the full 4π solid angle. Collecting these pairs can produce photon pairs at a rate of $\sim 10^{12}$ per second, given only moderate ensemble sizes of $\sim 10^6$ atoms.

The study of correlated/entangled photon pairs has long been a topic in the field of quantum optics [1]. The importance of paired photons is two-fold: they i) provide powerful tools to test the peculiar aspects of quantum mechanics, such as violations of local-realism [2, 3]; and ii) they hold promises for advancements in quantum measurement, communication, and information processing [4, 5, 6, 7, 8, 9, 10]. Over the past few decades, spontaneous parametric down-conversion (SPDC) in nonlinear crystals has been the standard source of photon pairs [11, 12]. More recently, an alternative class of biphoton sources has emerged, based on optical four-wave mixing (FWM) in atomic vapors [13, 14, 15, 16, 17, 18, 19, 20, 21]. These approaches rely on collective effects [22] to greatly increase the probability of correlated emission events. Compared to SPDC, photon pairs generated via FWM in general have a much narrower bandwidth, significantly greater temporal and spatial coherence, and much higher conversion efficiencies. They are thus particularly suitable for hybrid quantum communications and computations employing atoms and photons [10, 23], and for high-precision quantum measurements and imaging [5, 9].

This far, proposed FWM photon pair sources can be categorized into three types by level configuration. The first type, built on atomic two-level systems, is a connected double-Rayleigh emission process [24, 25]. Due to strong background Rayleigh scattering, however, the resulting pair correlation is very weak, without violating the necessary Cauchy criteria for biphoton correlation [17, 20]. A second type is configured on two-photon cascade emission in a four-level system [19, 26]. While high-fidelity photon pairs are generated, due to the unequal wavelengthes of two cascade photons, the phase-matching condition for collective emission can only be satisfied if the first photon is emitted by chance into a specific small solid-angle, thus unpaired emission dominates the overall radiation, resulting in a relatively low conversion efficiency. The third type employs Raman FWM (hereafter referred to as "RFWM") in multilevel systems, configured on double-Λ [13, 16, 17, 20, 21] or "X" [18] level diagrams. The major challenge in these schemes is to suppress background Rayleigh scattering,

which tends to rapidly overwhelm paired emission. Three approaches have been proposed to overcome this difficulty, including i) using frequency selectors to filter out Rayleigh photons [16]; ii) collecting pairs along emission directions where the dipole pattern leads to zero Rayleigh emission [17]; and iii) using a single-mode optical cavity to suppress Rayleigh transitions [18]. While yielding up to 10^5 pairs per second, all of these setups are unidirectional, where photon pairs are produced only along certain directions. This restricts the obtainable beam brightness of the photon pairs, since in each momentum mode, the time separation between pairs must be sufficiently large to achieve strong correlation effects. Lastly, in aforementioned FWM schemes where unpaired emissions dominate, atomic samples are rapidly thermalized due to random atomic recoils, limiting applications of these schemes to "hot" vapors only.

To substantially increase the gain rate and suppress the atomic thermalization, here we propose an omnidirectional biphoton source configured on a 'butterfly' level scheme. The central idea is to completely eliminate the background Rayleigh scattering in RFWM by employing electric-dipole forbidden driving channels. This can be accomplished using multiphoton pumping. Combining this with a Doppler-free geometry allows high-efficiency emission of photon pairs in the full 4π solid angle. Collecting these pairs will lead to twin beams of correlated or entangled photon pairs, whose brightness can be tens of thousands times greater than that via unidirectional schemes. Furthermore, since Rayleigh scattering has been eliminated, the atomic thermalization will be strongly suppressed, so that this scheme can also be applied to ultracold vapors including Bose-Einstein condensates (BECs).

A schematic level diagram of the butterfly scheme is shown in Fig. 1 (a). While greatly simplified with respect to a realistic level-scheme, this model will serve to illustrate the important dynamical effects. An atomic ensemble, initially prepared in the $|1\rangle$ state, is first weakly driven to the excited $|2\rangle$ level via a multi-photon pump process, which imparts a net recoil momentum of $\hbar\mathbf{K}$, so that for an initial momentum $\hbar\mathbf{k}_0$, an atom excited to $|2\rangle$ has a momentum of $\hbar(\mathbf{k}_0 + \mathbf{K})$. The atom then

spontaneously decays to $|3\rangle$, emitting a 'signal' photon with a random momentum $\hbar\mathbf{k}$, shifting the atom's momentum to $\hbar(\mathbf{k}_0 + \mathbf{K} - \mathbf{k})$. Decay to state $|1\rangle$, which would generate background Rayleigh scattering, is forbidden by dipole selection-rules. The atom in $|3\rangle$ state is then rapidly repumped to $|4\rangle$ by a strong multi-photon coupling process. The coupling is arranged to yield a net momentum of $-\hbar\mathbf{K}$, leading to a momentum of $\hbar(\mathbf{k}_0 - \mathbf{k})$ for the atom. From $|4\rangle$, the atom decays back to the $|1\rangle$ state, emitting an 'idler' photon, which will be emitted with momentum $-\hbar\mathbf{k}$ due to collective enhancement.

The collective enhancement mechanism can be understood by noting first that the emission of the signal photon with momentum $\hbar\mathbf{k}$ imprints 'which atom' information onto the atomic ensemble via atomic recoil, provided of course that the single-photon recoil momentum is larger than the momentum coherence length of the sample (which for a thermal gas of free particles is the inverse sample length). If the idler photon is then emitted with momentum $-\hbar\mathbf{k}$, the atom is restored to its initial momentum state of $\hbar\mathbf{k}_0$, thus 'erasing' the 'which atom' information, resulting in collective emission by all atoms within a wavelength of the emission axis, enhancing the emission rate by a factor $\sim n\lambda^2 R$, where n is the atomic density, $\lambda = 2\pi/|\mathbf{k}|$, and R is the cloud radius. The reason only this fraction of the atoms emit collectively is that the photons themselves carry sufficient information in their phase fronts to locate the transverse origin of emission with an accuracy given by the diffraction limit, λ. Conversely, emission of an 'idler' photon with a momentum other than $-\hbar\mathbf{k}$ is not collective, and is therefore suppressed by unitarity.

The fact that the driving and coupling pumps have opposite net momenta makes the scheme 'Doppler-free', so that phase-matched collective emission can occur regardless of which direction the signal photon randomly 'chooses', resulting in omni-directional emission of correlated photon pairs. This is clearly seen in Fig. 1 (b), where for an arbitrary $\mathbf{k}$, the atomic dynamics in the space of recoil momentum undergoes a closed, diamond-like cycle.

To study the system's dynamics, we quantize the electromagnetic field of signal and idler photons onto orthogonal collective-emission modes $\{|\mathbf{k}\rangle\}$. Each mode subtends a solid angle $\sim (\lambda/R)^2$, centered on $\mathbf{k}$, and the modes do not overlap. This quantization basis is mode matched to the collective emission angle. In this basis, the atomic dynamics is governed by a set of rate equations:

$$\frac{d}{dt}N_1 = \frac{i}{2}\left(\Omega_d \varrho_{21} - c.c\right) + \sum_{\mathbf{k}} \Gamma_4 \mu_{\mathbf{k}4} N_{\mathbf{k}4}(N_1 + 1), \quad (1)$$

$$\frac{d}{dt}N_2 = -\frac{i}{2}\left(\Omega_d \varrho_{21} - c.c\right) - \sum_{\mathbf{k}} \Gamma_2 \mu_{\mathbf{k}2} N_2(N_{\mathbf{k}3} + 1), (2)$$

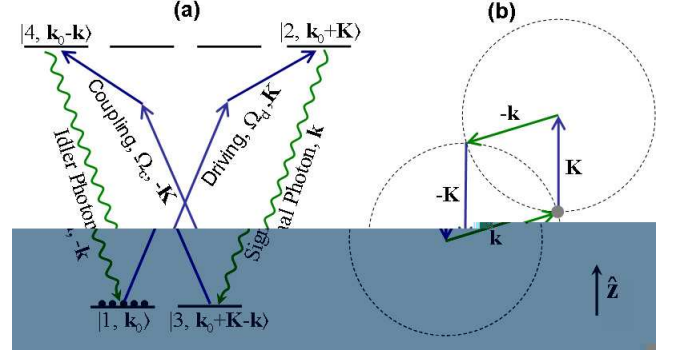$$\frac{d}{dt}\varrho_{21} = i\frac{\Omega_d}{2}(N_1 - N_2)$$

FIG. 1: (Color online) A schematic model of the butterfly scheme. Figure (a) draws the simplified level diagram, employing multi-photon driving and coupling pumps. The notation $|1, \mathbf{k}_0\rangle$ indicates a single atom state in level $|1\rangle$ and with momentum $\hbar\mathbf{k}_0$, and so on. Figure (b) shows a closed, diamond-like dynamical cycle in atom-recoil momentum space, for an arbitrary $\mathbf{k}$ of signal photons.

$$+ \frac{1}{2}\varrho_{21}\sum_{\mathbf{k}}\left[\Gamma_4 \mu_{\mathbf{k}4} N_{\mathbf{k}4} - \Gamma_2 \mu_{\mathbf{k}2}(N_{\mathbf{k}3} + 1)\right], \quad (3)$$

$$\frac{d}{dt}N_{\mathbf{k}3} = \frac{i}{2}\left(\Omega_c \varrho_{43} - c.c\right) + \Gamma_2 \mu_{\mathbf{k}2} N_2(N_{\mathbf{k}3} + 1), \quad (4)$$

$$\frac{d}{dt}N_{\mathbf{k}4} = -\frac{i}{2}\left(\Omega_c \varrho_{43} - c.c\right) - \Gamma_4 N_{\mathbf{k}4}(\mu_{\mathbf{k}4} N_1 + 1), \quad (5)$$

$$\frac{d}{dt}\varrho_{\mathbf{k}43} = i\frac{\Omega_c}{2}(N_{\mathbf{k}3} - N_{\mathbf{k}4})$$
$$+ \frac{1}{2}\varrho_{\mathbf{k}43}\left[\Gamma_2 \mu_{\mathbf{k}2} N_2 - \Gamma_4(\mu_{\mathbf{k}4} N_1 + 1)\right]. \quad (6)$$

Here, N_1 and N_2 are the atom numbers in states $|1\rangle$ and $|2\rangle$, and ϱ_{21} is the corresponding coherence term. $N_{\mathbf{k}3}$ is the number of atoms in $|3\rangle$, whose signal-photon recoil kick corresponds to emission into collective mode $|\mathbf{k}\rangle$. Similarly, $N_{\mathbf{k}4}$ is the number of these atoms transferred to the state $|4\rangle$ by the coupling laser and $\rho_{\mathbf{k}43}$ is the coherence between the two states. In the above equations, Γ_2, Γ_4 are the spontaneous emission rates for $|2\rangle \to |3\rangle$ and $|4\rangle \to |1\rangle$ decays, while $\mu_{\mathbf{k}2}$ and $\mu_{\mathbf{k}4}$ are the collective enhancement factors, which have been taken to be real. The imaginary part of $\mu_{\mathbf{k}2}, \mu_{\mathbf{k},4}$, describing the laser-induced dipole-dipole interaction, is in general orders of magnitude smaller than the real part, and can thus be neglected. For a spherical sample of radius R, we find $\mu_{\mathbf{k}j} = (1 - |\hat{k}\cdot\hat{d}_j|^2)\frac{3}{8\pi}\left(\frac{\lambda}{2R}\right)^2$. Here, $\hat{d}_2, \hat{d}_4$ are the unit vector directed along the dipole moments of the $|2\rangle \to |3\rangle$ and $|4\rangle \to |1\rangle$ transitions.

The total emission rates for signal and idler photons, corresponding to the (enhanced) decay rates of the $|2\rangle$ and $|4\rangle$ levels, are $R_S = \Gamma_2 \sum_{\mathbf{k}} \mu_{\mathbf{k}2} N_2(N_{\mathbf{k}3} + 1)$ and $R_I = \Gamma_4 \sum_{\mathbf{k}} \mu_{\mathbf{k}4} N_{\mathbf{k}4}(N_1 + 1)$, respectively. Assuming steady-state, clearly we must have $R_I \leq R_S$. If $R_I < R_S$, more signal photons are generated than idler photons, so that pairing is weak. Thus, at a minimum, strong pairing requires $R_I = R_S$. Focusing on a single $\hat{k}$ direction, and assuming $\mu_{\mathbf{k}2} = \mu_{\mathbf{k}4}$ and $\Gamma_2 = \Gamma_4$, we find

$\frac{R_I(\hat{k})}{R_S(\hat{k})} = \left(\frac{N_1+1}{N_2}\right)\left(\frac{N_{\mathbf{k}4}}{N_{\mathbf{k}3}+1}\right)$. For a strong drive, $\Omega_d \gtrsim \Gamma_2$, we have $N_2 \sim N_1$, so that we require $N_{\mathbf{k}4} \sim N_{\mathbf{k}3} \gg 1$, which thus requires a strong coupler, $\Omega_c \gtrsim \Gamma_4\mu_{\mathbf{k}4}N_1$, as well. We find that dynamically this doesn't work, instead population builds up in $N_{\mathbf{k}3}$ and $N_{\mathbf{k}4}$ without strong pairing. This leaves the case of weak driving, $\Omega_d \ll \Gamma_2$ so that $N_2 \ll N_1$. This then requires $N_{\mathbf{k}4} = \frac{N_2(N_{\mathbf{k}3}+1)}{N_1}$, which can be arranged by adjusting the drive and coupler strengths and detunings, and for $N_{\mathbf{k}4} \ll 1$ results in strong pairing.

The total number of photon pairs generated per second is given by $\Gamma_4 \sum_{\mathbf{k}} \mu_{\mathbf{k}4}N_{\mathbf{k}4}(N_1 + 1)$. For a BEC, the condensate atom loss rate, due to spontaneous emission from the $|4\rangle$ level, is $\Gamma_4 \sum_{\mathbf{k}} N_{\mathbf{k}4}$. The ratio of pair generation and atom loss rates is $\kappa = N_1\bar{\mu}$, where $\bar{\mu} = \sum_{\mathbf{k}} \mu_{\mathbf{k}4}N_{\mathbf{k}4}/\sum_{\mathbf{k}} N_{\mathbf{k}4}$. For a spherical sample this is roughly $\lambda^2/4\pi R^2$. Typically, κ is much greater than one, so that many pairs can be generated before rogue photon emission destroys the BEC. This means that if desired, a BEC can act as an ultra-bright photon-pair source without being destroyed in the process. We note that in general, an atom which emits spontaneously from $|4\rangle$ receives an additional photon recoil-kick, but is still fully able to participate in collective emission of subsequent photon pairs. In a more realistic level scheme this may not be true for atoms which spontaneously decay from $|4\rangle$ to a level other than $|1\rangle$.

To measure the time correlation of the two photons, we calculate the time-averaged second-order correlation function $g^{(2)}(\mathbf{k}, -\mathbf{k}, \tau)$ [2],

$$g^{(2)}(\mathbf{k},-\mathbf{k},\tau) = \frac{1}{T}\int_0^T dt \frac{\langle\hat{a}^{\dagger}_{\mathbf{k}s}(t)\hat{a}^{\dagger}_{-\mathbf{k}i}(t+\tau)\hat{a}_{-\mathbf{k}i}(t+\tau)\hat{a}_{\mathbf{k}s}(t)\rangle}{\langle\hat{a}^{\dagger}_{\mathbf{k}s}(t)\hat{a}_{\mathbf{k}s}(t)\rangle\langle\hat{a}^{\dagger}_{-\mathbf{k}i}(t+\tau)\hat{a}_{-\mathbf{k}i}(t+\tau)\rangle},$$

where $\hat{a}_{\mathbf{k}s}$ and $\hat{a}_{\mathbf{k}i}$ are the annihilation operators for signal and idler photons, which may or may not differ in polarization for a given $\mathbf{k}$, and T is the averaging window. This is evaluated by first using adiabatic following to write the photon operators in terms of the atomic operators. The resulting expressions are then factorized into products of the occupation numbers. The equations for the occupation numbers are solved in steady-state with atom losses neglected, which allows us to take $T \to \infty$. In this manner, we find to a good approximation that, $g^{(2)}(\mathbf{k}, -\mathbf{k}, \tau) \approx 1 + \frac{1}{N_{\mathbf{k}4}}\chi(\tau)$. For a strong coupling with $\Omega_c \gtrsim \Gamma_4\mu_{\mathbf{k}4}N_1$, we find $\chi(\tau) \approx \sin^2\left(\frac{1}{2}\Omega_c\tau\right)\exp(-\frac{1}{2}\Gamma_4\mu_{\mathbf{k}4}N_1\tau)$. The correlation then exhibits oscillatory and damped behavior with sharp peaks, indicating strong time-correlation between the signal and idler photons [16]. The time delay of idler photons is roughly $(\Gamma_4\mu_{\mathbf{k}}N_1)^{-1}$, which is much shorter than the temporal coherence length of the signal photons. This ensures strong interferences of paired photons, for example, when mixed in a polarized beamsplitter [18].

As an example, we solve the rate-equation dynamics for a symmetric Gaussian sample of $N = 10^6$ atoms. We consider resonant driving and coupling pumps propagating along $\hat{z}$ and $-\hat{z}$ directions, and assume $\Gamma_2 = \Gamma_4 \equiv \Gamma$.
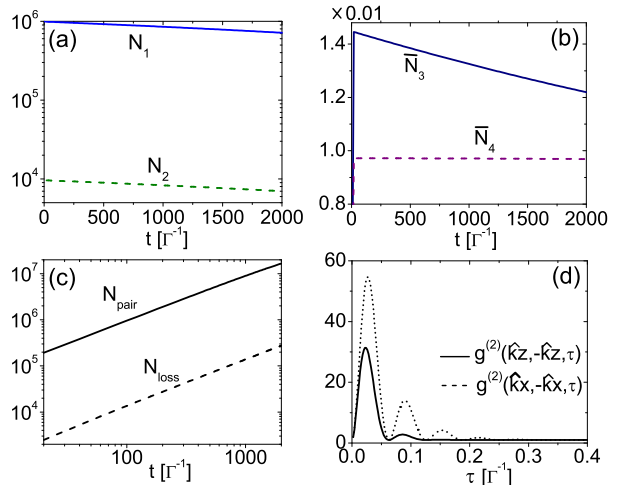
FIG. 2: (Color online) Figures (a)-(b) show the evolutions of $N_1, N_2, \overline{N}_3, \overline{N}_4$, while (c) compares the number of generated photon pairs N_{pair} and lost atoms N_{loss}. Figure (d) plots the second-order correlation function $g^{(2)}(\mathbf{k}, -\mathbf{k}, \tau)$ for $\mathbf{k} = k\hat{z}$ and $\mathbf{k} = k\hat{x}$, respectively. Parameters are given in text.

We choose $\Omega_d = 0.1\Gamma$, $\Omega_c = 100\Gamma$ and $R = 50\lambda$. The results are shown in Fig. 2 (a)-(d). In figure (a), we plot the time evolutions of N_1, N_2, showing that at all times only a small fraction of atoms are excited, as required. In figure (b), we plot the average occupation numbers $\overline{N}_3$ and $\overline{N}_4$, obtained by averaging over $\mathbf{k}$. Both are found to be of order of 0.01, so that there is negligible overlap between subsequent pairs in a given mode $\mathbf{k}$. The total photon-pair number and lost atom number are shown in figure (c), where they are found to increase linearly in time with fitted rates of $8.3 \times 10^3\Gamma$ and $1.4 \times 10^2\Gamma$. In figure (d), we plot the second-order correlation functions for photon pairs propagating along $\pm\hat{z}$ and $\pm\hat{x}$ directions. Both cases exhibit sharp peaks of widths $\sim 0.05\Gamma^{-1}$, indicating strong temporal correlation which violate the standard Cauchy-Schwartz inequality by a factor $\gtrsim 1000$.

We now examine the polarization entanglement of paired photons. For $\hat{d}_{2,4} = \frac{1}{\sqrt{2}}(\hat{x} \pm i\hat{y})$, the probabilities for signal photons to be left(right) circularly polarized along $\mathbf{k}$, denoted $\hat{\epsilon}_L(\hat{\epsilon}_R)$, are $\beta_S^L(\theta) = \left(1 + \cot^4\frac{\theta}{2}\right)^{-1}$ and $\beta_S^R(\theta) = \beta_S^L(\pi - \theta)$, with θ defined relative to $\mathbf{K}$. Similarly, for the idler photons we have $\beta_I^R = \beta_S^L(\theta)$, and $\beta_I^L = \beta_S^R(\theta)$. The probability for photons to be in opposite circular polarizations along $\mathbf{k}$ (thus in the same polarizations along each's propagating direction) is $P(\theta) = (1 + \cot^8\frac{\theta}{2})/\left(1 + \cot^4\frac{\theta}{2}\right)^2$, which is extremely flat around $\theta = 0, \pi$, where $P(\theta) \approx 1 - \frac{1}{8}\text{mod}(\theta, \pi)^4 \approx 1$, meaning that photon pairs emitted over a wide range of θ will yield strong polarization entanglement. Due to the temporal overlap of signal and idler photons, each pair
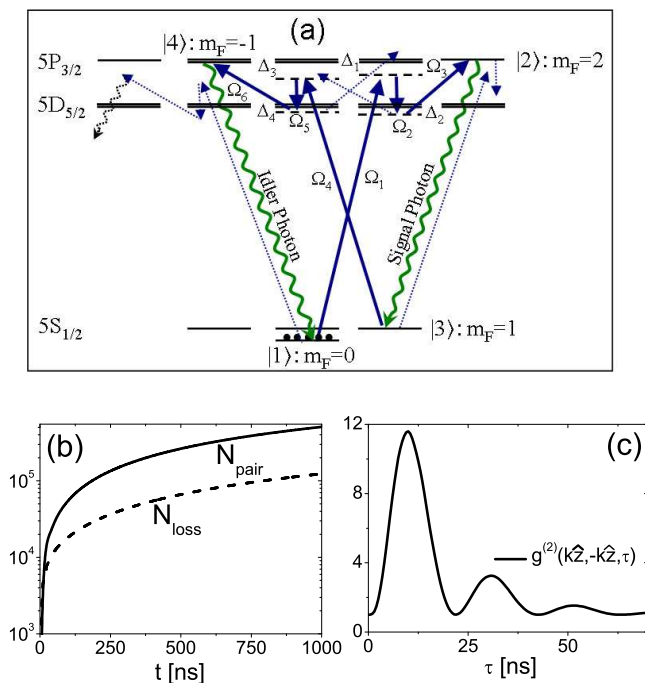
FIG. 3: (Color online) A realistic butterfly scheme using Ag atoms. Figure (a) shows the level diagram, where thicker solid lines draw dominating coupling channels, while thinner dashed lines show weaker side transitions. Figure (b) plots the time evolutions of N_{pair} and N_{loss}, while (c) draws the time correlation function for photon pairs emitted along $\pm\hat{z}$ directions.

emitted within the strong correlation angle is approximately in the Bell state of $|\Psi^+\rangle = \frac{1}{\sqrt{2}}(|\epsilon_R\epsilon_L\rangle + |\epsilon_L\epsilon_R\rangle)$. For example, pairs with one photon emitted within $\theta < 0.5$ (corresponding to 17% of the emitted pairs) have an entanglement fidelity $\geq 99\%$.

We now consider a realistic butterfly level scheme configured on the 328nm-line of the $5^2S_{1/2} \leftrightarrow 5^2P_{3/2}$ transition in Silver, as shown in figure 3 (a). The atoms are prepared in the $|1\rangle \equiv |F = 0, m_F = 0\rangle$ state and then follow a FWM cycle which deposits them in level $|3\rangle$. A second independent FWM cycle then returns them to the initial $|1\rangle$ state. The drive (coupling) FWM cycle consists of one UV laser, and two infrared lasers, with Rabi

frequencies $\Omega_{1(4)}$ $\Omega_{2(5)}$ and $\Omega_{3(6)}$, respectively. Signal photons are emitted as $|2\rangle$ atoms spontaneously decay to the sole dipole-allowed state of $|3\rangle \equiv |F = 1, m_F = 1\rangle$, and idler photons are generated as each atom in $|4\rangle$ (actually 2 effectively degenerate hyperfine levels) decays collectively back to $|1\rangle$, and to its initial momentum $\hbar\mathbf{k}_0$ (atoms which spontaneously decay to other hyperfine levels are 'lost' as they can no longer participate in the collective emission cycle). We note that the frequencies of the signal and idler photons differ by the ground hyperfine splitting, which is smaller than the superradiance-broadened linewidth of the idler photons, thus guaranteeing the frequency indistinguishability of the photons.

For a spherical cloud of 10^6 atoms with a radius of $R = 20\mu m$, and with (all in units of GHz): $\Omega_1 = 0.4$, $\Omega_2 = 9$, $\Omega_3 = 1.5$, $\Omega_4 = 4$, $\Omega_5 = 12$, $\Omega_6 = 0.5$, $\Delta_1 = 24$, $\Delta_2 = 3$, $\Delta_3 = 80$, $\Delta_4 = 0.4$, we solve the rate equations numerically. Results are shown in figure 3 (b) and (c). In figure (b), the production rate of photon pairs is $\sim 0.5 \times 10^{12}$ per second. The ratio of generated pairs N_{pair} to lost atoms N_{loss} is about 4, so that roughly 10^6 pairs of photons can be generated before significant atomic loss. In figure (c), the time correlation function exhibits sharp peaks, thus showing strong pair correlation between signal and idler photons.

The dominant loss mechanism is due to atoms from $|1\rangle$ being pumped to $|4\rangle$ by Ω_4, and then decaying non-collectively. Due the the detuning of this mechanism, the rogue photons are different in frequency from signal and idler photons by ~ 80 GHz, which can be filtered out. When the atom loss becomes significant, the system will enter a more complicated regime, where the system tries to equilibrate, resulting in macroscopic occupation of all ground hyperfine sub-levels, and presumably diminished pair correlations. If this is the case, then only a small number of photon pairs will be generated, but in a very short burst. In this case, this particular system may be an excellent source for generating highly number-difference squeezed twin beams for quantum interferometry.

[1] D. Bouwmeester, A. Ekert, and A. Zeilinger, *The Physics of Quantum information* (Springer-Verlag, Berlin, 2000).
[2] M. O. Scully and M. S. Zubairy, *Quantum Optics* (Cambridge University Press, NewYork, USA, 1997).
[3] S. Gröblacher et. al, Nature **446**, 871 (2007).
[4] D. Bouwmeester, J.-W. Pan, K. Mattle, M. Eibl, H. Weinfurter, and A. Zeilinger, Nature **390**, 575 (1997).
[5] A. Migdall, R. Datla, A. Sergienko, J. S. Orszak, and Y. H. Shih, Appl. Opt. **37**, 3455 (1998).
[6] M. D. Lukin, Rev. Mod. Phys. **75**, 457 (2003).
[7] M. Fleischhauer, A. Imamoglu, and J. P. Marangos, Rev. Mod. Phys **77**, 633 (2005).
[8] J. F. Sherson, H. Krauter, R. K. Olsson, B. Julsgaard, K. Hammerer, I. Cirac, and E. S. Polzik, Nature **443**, 557 (2006).
[9] V. Boyer, M. A. Marino, R. C. Pooser, and P. D. Lett, Science **321**, 544 (2008).
[10] H. J. Kimble, Nature **453**, 1023 (2008).
[11] S. E. Harris, M. K. Oshman, and R. L. Byer, Phys. Rev. Lett. **18**, 732 (1967).
[12] F. König, E. J. Mason, F. N. C. Wong, and M. A. Albota, Phys. Rev. A **71**, 033805 (2005).

[13] A. S. Zibrov, M. D. Lukin, and M. O. Scully, Phys. Rev. Lett. **83**, 4049 (1999).

[14] C. H. van der Wal, M. D. Eisamen, A. Andre, R. L. Walsworth, D. F. Phyillips, A. S. Zibrov, and M. D. Lukin, Science **301**, 196 (2003).

[15] A. Kuzmich, W. P. Bowen, A. D. Boozer, A. Boca, C. W. Chou, L. M. Duan, and H. J. Kimble, Nature **423**, 731 (2003).

[16] V. Balić, D. A. Braje, P. Kolchin, G. Y. Yin, and S. E. Harris, Phys. Rev. Lett. **94**, 183601 (2005).

[17] P. Kolchin, S. Du, C. Belthangady, G. Y. Yin, and S. E. Harris, Phys. Rev. Lett. **97**, 113602 (2006).

[18] J. Thompson, J. Simon, H. Loh, and V. Vuletic, Science **313**, 74 (2006).

[19] T. Chanelière, D. N. Matsukevich, S. D. Jenkins, T. A. B. Kennedy, M. S. Chapman, and A. Kuzmich, Phys. Rev. Lett. **96**, 093604 (2006).

[20] S. Du, J. Wen, M. H. Rubin, and G. Y. Yin, Phys. Rev. Lett. **98**, 053601 (2007).

[21] S. Du, P. Kolchin, C. Belthangady, G. Y. Yin, and S. E. Harris, Phys. Rev. Lett. **100**, 183603 (2008).

[22] R. H. Dicke, Phys. Rev. **93**, 99 (1954).

[23] L. M. Duan, M. D. Lukin, J. I. Cirac, and P. Zoller, Nature **414**, 413 (2001).

[24] A. Aspect, G. Roger, S. Reynaud, J. Dalibard, and C. Cohen-Tannoudji, Phys. Rev. Lett. **45**, 617 (1980).

[25] P. Grangier, G. Roger, A. Aspect, A. Heidmann, and S. Reynaud, Phys. Rev. Lett. **57**, 687 (1986).

[26] C. H. R. Ooi and M. O. Scully, Phys. Rev. A **76**, 043822 (2007).